Progress In Electromagnetics Research, Vol. 119, 497–511, 2011

HIGH SELECTIVITY AND CONTROLLABILITY OF A PARALLEL-PLATE COMPONENT WITH A FILLED RECTANGULAR RIDGE

C. A. Valagiannopoulos*

Department of Radio Science and Engineering, School of Electrical Engineering, Aalto University, 5A Otakaari St., Espoo, FIN-02150, Finland

Abstract—Achieving and controlling highly selective response in an electronic component could be particularly beneficial for numerous practical applications. In this work, we consider a simple configuration of a discontinuous parallel-plate waveguide with a narrow rectangular ridge filled with axially anisotropic material. The formulated boundary value problem is rigorously treated with help from mode matching technique. The variables with respect to which the device exhibits highly selective behavior and the parameters through which the regulation of sharp variations becomes possible, have been identified. Several graphs demonstrating these properties are analyzed and discussed.

1. INTRODUCTION

The functionality of an electromagnetic device is determined by the configuration of its components and its primary external excitation. When two almost identical structures (with slightly different constituent parameters) react very differently under the same excitation or, alternatively, when the output of a single device is very sensitive to its own input, then we have systems with highly selective response. Such a feature is exploited in numerous practical applications because it increases the discernibility of very similar entities and provide each one with a unique identity characteristic. Radio frequency identification (RFID) technologies extensively utilize resonant circuits, with high selectivity properties, in electronic tags attached to objects

Received 26 June 2011, Accepted 19 August 2011, Scheduled 27 August 2011
* Corresponding author: Constantinos A. Valagiannopoulos (konstantinos.valagiannopoulos@aalto.fi).

for the purpose of tracking. In particular, it has been shown that advanced RFID performance may be achieved by means of low-cost batteryless devices with highly selective transfer functions [1]. Also, the design of passive RFID tags is facilitated by components with selective correlation between input and output [2]. In addition, similar networks are utilized in commercial applications for detecting the originality of purchased brand products and commodities. Low cost and environmentally friendly wireless sensors have already been developed based on systems with selective response [3]. The idea of electromagnetic selectivity has been examined in numerous recent reports ([4–18]).

The aforementioned devices mainly incorporate printed circuit boards (PCBs) that mechanically support and electrically connect electronic components using conductive pathways, tracks or signal traces etched from copper sheets laminated onto dielectric substrates. Printed circuit boards are used in virtually all commercially-produced electronic devices due to their inherent advantages discussed in [19]. In particular, PCBs are inexpensive, highly reliable and simultaneously very fast for high-volume automated production. Within these structures, discontinuous coplanar waveguides are created between the metallic patches and the conducting sheets. These waveguide discontinuities have been investigated for many decades due to their susceptibility to analytical treatments [20]. For example, a circular cylinder in the vicinity of a step discontinuity in a parallel-plate waveguide, is analyzed through an integral equation formulation [21]. Furthermore, the Green's function of a coplanar waveguide with multiple discontinuities has been computed in compact form with help from mode matching technique [22]. Waveguides and similar devices have been also investigated in many other works and studies ([23–37]).

In this work, we consider a parallel-plate waveguide which changes abruptly its height at a narrow gap filled with an axially anisotropic material. The small longitudinal size of the discontinuity and its anisotropic filling reinforce the controlling capability of this intermediate component. We apply a semi-analytical method of mode matching and the obtained result differs little from the unique solution of the boundary value problem. To verify our approach, we have performed extensive and successful tests of the boundary conditions, which are not included, in the present study, for brevity. The response of the device is represented with respect to the excitation or configuration parameters of the problem and several cases with abrupt extrema have been noted. The regulating role of the input variables in shifting these sharp variations of the system output has been also investigated. Accordingly, certain conclusions for achieving

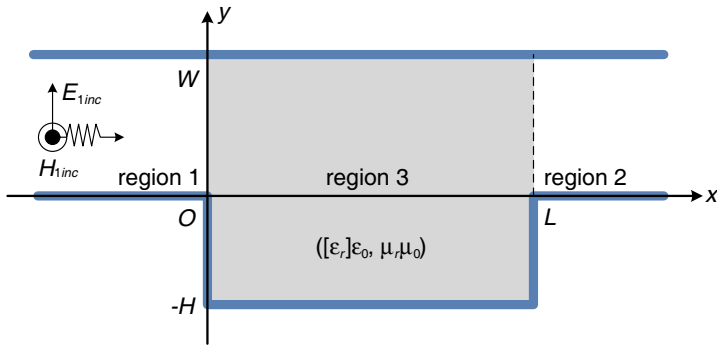

Figure 1. The configuration of the investigated discontinuous waveguide.

and controlling high selectivity in such a simple passive structure, have been extracted. The novelty of the results and the approach lies in the fact that the specific type of configuration has not been examined with these particular purposes.

2. MATHEMATICAL ANALYSIS

2.1. Problem Definition

In Figure 1, one can inspect the physical configuration of the examined device and the employed Cartesian coordinate system $(x,\ y,\ z)$. An empty parallel-plate waveguide of height W is separated into two regions (1 and 2) by a component (region 3) of length L and height $(H + W)$, filled with an arbitrary axially anisotropic substance possessing the following relative permittivity tensor:

$$[\epsilon_r] = \begin{bmatrix} \epsilon_{rx} & 0 & 0 \\ 0 & \epsilon_{ry} & 0 \\ 0 & 0 & \epsilon_{rz} \end{bmatrix} \tag{1}$$

and relative magnetic permeability μ_r. In other words, two step discontinuities are formed at $x = 0,\ L$ by a rectangular metallic well, occupying the area: $\{0 < x < L, -H < y < 0\}$. The harmonic time dependence $e^{+j2\pi ft}$ is suppressed throughout the analysis, while the structure is excited by a $\mathbf{y}$-polarized wave of unitary electric field $\mathbf{E}_{1,inc} = \mathbf{y}e^{-jk_0x}$ propagating along the positive $\mathbf{x}$ semi-axis, namely the basic mode of the parallel-plate waveguide. This type of excitation has been chosen in order to outline a nontrivial role for the discontinuity ridge through the parameter ϵ_{rx}. Note that, in

the absence of the well ($H = 0$), fields of this polarization do not interact at all with the horizontal characteristics (dielectric constant along $\mathbf{x}$ axis) of the filling anisotropic substance. The notation $k_0 = 2\pi f\sqrt{\epsilon_0\mu_0} = 2\pi f/c$, where $c = 3 \cdot 10^8$ m/sec, is reserved for the free-space wavenumber.

Selectivity should not be confused with instabilities occurring when the system acquires a positive Lyapunov exponent and becomes very sensitive to initial conditions. Instability is an unwanted feature of any functional system contrary to selectivity which can have many beneficial aspects. In particular, the selective response is manipulable directly through the system parameters and could be realized with high accuracy for specific applications. In this sense, the careful selection of the input variables, determines directly the characteristics of the developed resonance. Therefore, the scope of this work is to identify certain variables and value ranges, for the considered simple model, with respect to which the response of the system is not only highly selective but also easily controllable.

2.2. Field Formulas

Due to the presence of the corrugations, the reflected electric field into region 1 and the transmitting one into region 2, would certainly possess a longitudinal ($\mathbf{x}$) component as follows:

$$\mathbf{E}_{1,ref} = \sum_{n=0}^{+\infty} R_1(n) \left[n\pi \sin\left(\frac{n\pi y}{W}\right) \mathbf{x} + j\beta_n W \cos\left(\frac{n\pi y}{W}\right) \mathbf{y} \right] e^{j\beta_n x}, \quad (2)$$

$$\mathbf{E}_2 = \sum_{n=0}^{+\infty} T_2(n) \left[n\pi \sin\left(\frac{n\pi y}{W}\right) \mathbf{x} - j\beta_n W \cos\left(\frac{n\pi y}{W}\right) \mathbf{y} \right] e^{-j\beta_n (x-L)}. \quad (3)$$

Note that $\beta_n = \sqrt{k_0^2 - (\frac{n\pi}{W})^2}$ with $\Re[\beta_n] \geq 0$ and $\Im[\beta_n] \leq 0$. Similarly, the electric field into region 3, is given by:

$$\mathbf{E}_3 = \sum_{n=0}^{+\infty} \left\{ \frac{\epsilon_{ry}}{\epsilon_{rx}} n\pi \sin\left(\frac{n\pi(y-W)}{H+W}\right) \left[e^{-j\gamma_n x} T_3(n) + e^{j\gamma_n x} R_3(n) \right] \mathbf{x} \right.$$
$$\left. - j\gamma_n (H+W) \cos\left(\frac{n\pi(y-W)}{H+W}\right) \left[e^{-j\gamma_n x} T_3(n) - e^{j\gamma_n x} R_3(n) \right] \mathbf{y} \right\}, \quad (4)$$

where $\gamma_n = \sqrt{\frac{\epsilon_{ry}}{\epsilon_{rx}} [k_0^2 \epsilon_{rx} \mu_r - (\frac{n\pi}{H+W})^2]}$ evaluated with $\Re[\gamma_n] \geq 0$ and $\Im[\gamma_n] \leq 0$. Obviously, the magnetic fields $\{\mathbf{H}_{1,inc}, \mathbf{H}_{1,ref}, \mathbf{H}_2, \mathbf{H}_3\}$ possess a single component parallel to $\mathbf{z}$ axis. All the functions are dependent on the spatial arguments (x, y).

2.3. Mode Matching

The boundary conditions concerning the continuity of the tangential electric components at the planes $x = 0$, L, are written as:

$$\mathbf{y} \cdot \mathbf{E}_3(0,y) = \begin{cases} 0, & -H < y < 0 \\ \mathbf{y} \cdot [\mathbf{E}_{1,inc}(0,y) + \mathbf{E}_{1,ref}(0,y)], & 0 < y < W \end{cases}, \quad (5)$$

$$\mathbf{y} \cdot \mathbf{E}_3(L,y) = \begin{cases} 0, & -H < y < 0 \\ \mathbf{y} \cdot \mathbf{E}_2(L,y), & 0 < y < W \end{cases}. \quad (6)$$

Both equations are referring to the range $y \in (-H, W)$ and thus we act on them with the operator: $\int_{-H}^{W} \star \cos(\frac{m\pi(y-W)}{H+W})dy$ for $m \in \mathbb{N}$. The magnetic boundary conditions are written as: $\mathbf{z} \cdot [\mathbf{H}_3(0,y) - \mathbf{H}_{1,inc}(0,y) - \mathbf{H}_{1,ref}(0,y)] = 0$ and $\mathbf{z} \cdot [\mathbf{H}_3(L,y) - \mathbf{H}_2(L,y)] = 0$ and they are projected on the function set $\{\cos(\frac{m\pi y}{W}),\ m \in \mathbb{N}\}$ as being valid along the interval $0 < y < W$.

Once the integrations are carried out analytically, the following linear system is obtained:

$$\begin{bmatrix} \mathbf{A} & \bar{\mathbf{D}}' & \mathbf{D}' & \mathbf{O} \\ \mathbf{D} & \mathbf{B} & \mathbf{B} & \mathbf{O} \\ \mathbf{O} & \bar{\mathbf{D}}'' & \mathbf{D}'' & \bar{\mathbf{A}} \\ \mathbf{O} & \bar{\mathbf{C}} & \mathbf{C} & \mathbf{D} \end{bmatrix} \cdot \begin{bmatrix} \mathbf{r}_1 \\ \mathbf{t}_3 \\ \mathbf{r}_3 \\ \mathbf{t}_2 \end{bmatrix} = \begin{bmatrix} \mathbf{u} \\ \mathbf{v} \\ 0 \\ 0 \end{bmatrix}, \quad (7)$$

where $\{\mathbf{r}_1, \mathbf{t}_3, \mathbf{r}_3, \mathbf{t}_2\}$ are the related vectors of the unknown coefficients $\{R_1(m), T_3(m), R_3(m), T_2(m),\ m \in \mathbb{N}\}$ and $\bar{z}$ equals the complex quantity z if one replaces the isolated imaginary units j with their opposite. To define the diagonal matrices $\mathbf{D}$, $\mathbf{D}'$, $\mathbf{D}''$, we use the notation diag$[q_m,\ m \in \mathbb{N}]$, where $\{q_m,\ m \in \mathbb{N}\}$ are its nonzero diagonal elements. In particular:

$$\mathbf{D} = \frac{W}{2}\text{diag}\left[(-1)^m(1+\delta_{m0}),\ m \in \mathbb{N}\right], \quad (8)$$

$$\mathbf{D}' = j\frac{H+W}{2}\text{diag}\left[\gamma_m(1+\delta_{m0}),\ m \in \mathbb{N}\right], \quad (9)$$

$$\mathbf{D}'' = j\frac{H+W}{2}\text{diag}\left[e^{j\gamma_m L}\gamma_m(1+\delta_{m0}),\ m \in \mathbb{N}\right], \quad (10)$$

where the symbol δ is used for the Kronecker delta. The elements positioned at the m-th row and n-th column of the matrices $\mathbf{A}, \mathbf{B}, \mathbf{C}$, are defined as follows:

$$A(m,n) = j\beta_n F(m,n), \quad (11)$$

$$B(m,n) = \epsilon_{ry}(-1)^m F(n,m), \quad (12)$$

$$C(m,n) = \epsilon_{ry}e^{j\gamma_n L}(-1)^m F(n,m), \quad (13)$$

where the auxiliary quantity $F(m,n)$ is :

$$F(m,n)=\frac{W^2(H+W)}{\pi}\frac{m\sin\left(\frac{m\pi W}{H+W}\right)}{n^2(H+W)^2-m^2W^2}. \tag{14}$$

The m-th elements of the constant vectors $\mathbf{u}$, $\mathbf{v}$ of the linear system, are given by:

$$u(m) = \frac{H+W}{\pi}\frac{\sin\left(\frac{m\pi W}{H+W}\right)}{m}, \tag{15}$$

$$v(m) = -j\frac{W}{k_0}\delta_{m0}. \tag{16}$$

The symbols $\mathbf{O}$, 0 represent the zero matrix and vector respectively. In case one truncates properly the series (2), (3), (4), the unknown coefficients are determined by inverting the matrix of the system (7) which is numerically stable due to the "Galerkin projection" feature of the mode matching method ([38, 39]).

3. NUMERICAL RESULTS

3.1. Input and Output Quantities

Prior to proceeding with the discussion of the graphs, the value ranges of the input parameters should be clarified in the first place. The operating frequencies are chosen within the microwave band: $1\,\text{GHz} < f < 10\,\text{GHz}$, which are commonly used in exciting coplanar waveguides of a typical electromagnetics laboratory. The height W is kept fixed at 20 mm throughout the simulations, so that a single-mode propagation is permitted. The length L is much smaller than W to sharpen the effect of the discontinuity. In other words, the controlling utility of the ridge's depth H would be reinforced when $L \to 0$; in most cases, the vast portion of the incident power would pass to the other side, and thus abrupt, isolated extrema in the response of the device, would appear more easily. The material's constituent parameters cover the following negative and positive real values: $-5 < \epsilon_{rx}, \epsilon_{ry}, \mu_r < 5$. Due to the nature of the excitation, the parameter ϵ_{rz} does not participate in the algebraic operations and thus is absent from our considerations. The depth H can increase arbitrarily to retain its regulating role. Obviously, the truncation limit N of the series, defining the mode matching solutions, is chosen high enough to obtain convergent results in every single case. However, validation results are not included here for brevity; in any case, the numerical implementation is well-known and straightforward. We have chosen a configuration that stability

and accuracy is easily achieved, unlike more complicated ones (for example if the anisotropic substance occupied only the well region $\{0 < x < L, -H < y < 0\}$), where complex roots of transcendental equations [43] would be required.

The scattering parameters for the considered two-port network are given by [21]:

$$S_{11} = \lim_{x\to-\infty} \frac{\mathbf{y}\cdot\mathbf{E}_{1,ref}(x,y)}{\mathbf{y}\cdot\mathbf{E}_{1,inc}(x,y)} = jk_0R_1(0), \tag{17}$$

$$S_{21} = \lim_{x\to+\infty} \frac{\mathbf{y}\cdot\mathbf{E}_2(x,y)}{\mathbf{y}\cdot\mathbf{E}_{1,inc}(x,y)} = -jk_0e^{jk_0L}T_2(0), \tag{18}$$

when only the basic ($n = 0$) mode of the waveguide is propagating. The preservation of energy expressed from the equation $|S_{11}|^2 + |S_{21}|^2 = 1$ has been checked successfully, each time the aforementioned method is implemented. The input impedance of the device, when the load is open-circuited, reads [41]:

$$Z_{in} = -\frac{1+S_{11}}{S_{11}}\zeta_0, \tag{19}$$

where $\zeta_0 = 120\pi\,\Omega$ is the wave impedance into free space which is identical to the reference impedance of the basic mode of the waveguide. The magnitudes of the transmission coefficient $|S_{21}|$ and the normalized input impedance $|Z_{in}|/\zeta_0$ are the characteristic

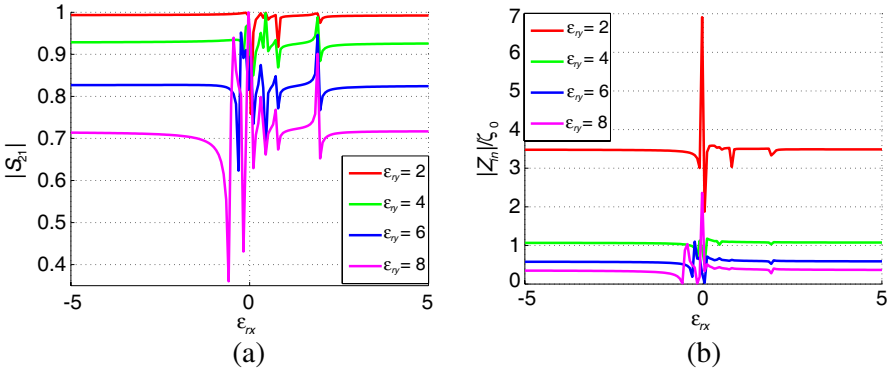

Figure 2. The magnitude of: (a) the transmission coefficient and (b) the normalized input impedance of the two-port network as functions of the permittivity ϵ_{rx} for various permittivities ϵ_{ry} of the filling material. Plot parameters: $W = 20\,\text{mm}$, $L = 2\,\text{mm}$, $\mu_r = 1$, $H = 40\,\text{mm}$, $f = 0.99\frac{c}{2W}$.

quantities of the device; thus, their variations with respect to the problem parameters are shown and discussed in the following.

3.2. Graphs Discussion

In Figure 2(a), we represent the transfer function of the waveguide with respect to the permittivity ϵ_{rx} for several different ϵ_{ry}. One can observe a remarkable stability for larger $|\epsilon_{rx}|$ at both the ends of the diagram and also rapid fluctuations in the middle of it. The curves are oscillating more abruptly and around higher average levels for decreasing ϵ_{ry} (e.g., $|S_{21}| \cong 1$ for $\epsilon_{ry} = 2$). Mind also that the resonances happen at almost the same values of ϵ_{rx}, regardless of the dielectric constant ϵ_{ry}. Consequently, the parameter ϵ_{rx} is highly selective, while the transmission is controllable through parameter ϵ_{ry}. In Figure 2(b), the magnitude of the normalized input impedance of the device is shown for the same configuration. The permittivity ϵ_{ry} is inversely related to the input impedance which is natural since materials with large dielectric constants imitate the behavior of metallic conductors. Again, we notice fast changes of the recorded quantity in the vicinity of $\epsilon_{rx} = 0$ at the "low-index metamaterial" (LIM) or "ϵ near to zero" (ENZ) regime [42], while the response remains almost unaltered along the rest of the horizontal axis. Especially for the $\epsilon_{ry} = 4$ case, the input impedance equals the characteristic one of the vacuum for practically any value of the

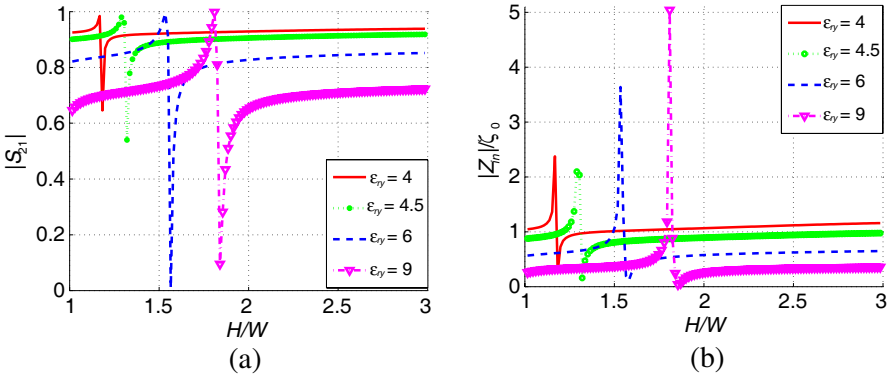

Figure 3. The magnitude of: (a) the transmission coefficient and (b) the normalized input impedance of the two-port network as functions of the depth of the well for various permittivities ϵ_{ry} of the filling material. Plot parameters: $W = 20\,\text{mm}$, $L = 2\,\text{mm}$, $\epsilon_r = -5$, $\mu_r = 1$, $f = 0.99\frac{c}{2W}$.

dielectric constant ϵ_{rx}. When that LIM/ENZ limit is reached, the filling material neutralizes the electric forces, yielding to negligible electric flux densities along the horizontal direction. This fact combined with the vanishing tangential component along the edges, makes the transmission very sensitive to the permittivity parameters.

In Figure 3(a), we represent the transfer function of the two-port network with respect to the normalized height of the ridge H/W for various dielectric constants ϵ_{ry}, of a metamaterial ($\epsilon_{rx} = -5$). We notice sharp resonances at moderate heights $H < 2W$ which increase for higher permittivities. In addition, the quantity variation in the vicinity of each resonance is more substantial when ϵ_{ry} gets larger. It is also remarkable that for larger H/W, the response $|S_{21}|$ tends to a constant value inversely related to the parameter ϵ_{ry}. Similar conclusions stand for Figure 3(b), where the normalized input impedance is shown for the identical case. At the same points of the horizontal axis, we notice "spikes" for $|Z_{in}|/\zeta_0$ getting more substantial for larger ϵ_{ry}, which leads to lower minima ($|Z_{in}| \to 0$ for $\epsilon_{ry} = 9$ in the vicinity of the resonance) and smaller final quantity (when $H/W \to \infty$). Evidently, we identify another factor (H/W) that could, at moderate values, selectively change the response of the network and we remark again the regulating role of the dielectric constant ϵ_{ry} in operating the device. Note that when the depth of the well is increasing, more modes from (2), (3), (4) are required to achieve zero field along the edges. Therefore, the resonances are attributed to strong inter-mode scattering occurred for specific values of H/W.

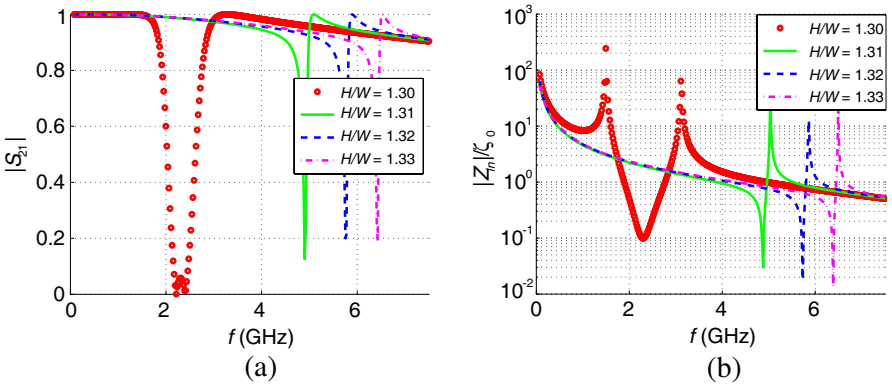

Figure 4. The magnitude of: (a) the transmission coefficient and (b) the normalized input impedance of the two-port network as functions of the operating frequency for various normalized depths of the well. Plot parameters: $W = 20\,\text{mm}$, $L = 2\,\text{mm}$, $\epsilon_{rx} = -5$, $\epsilon_{ry} = 6$, $\mu_r = 2$.

In Figure 4(a), we show the magnitude of the transmission coefficient as function of the operating frequency for four different but similar normalized depths H/W of the well. By inspecting the diagram, one clearly notices the respective resonances for each of the examined cases which appear at higher frequencies and get more narrow for increasing H/W. In particular, the resonance for the case of $H/W = 1.3$ is so wide that includes a minor variation of $|S_{21}|$ corresponding to two minima very close each other. Notice also that for smaller heights H/W, there are deeper declines that reaches at lower points ($|S_{21}| \to 0$ for $H/W = 1.3$ in the vicinity of the resonance). In Figure 4(b), the relative input impedance of the network is represented in a logarithmic plot for the aforementioned configurations. As happens in Figure 4(a), the input impedance tends to the same values for smaller and larger frequencies regardless of the choice of the depth. Moreover, at the same resonant frequencies as in Figure 4(a), which are directly dependent on H/W, the impedance $|Z_{in}|$ reaches a minimum and then abruptly attains very high magnitudes of several thousands Ω ($|Z_{in}|/\zeta_0 > 300$). Once more, we can notice the highly selective effect of the depth H/W, with respect to the oscillation frequency as well. The sharp variations of the device's output response are typical resonances as those observed in common antenna and waveguide structures [44].

In Figure 5(a), the magnitude of the transmission coefficient $|S_{21}|$ is represented in contour plot with respect to the normalized depth H/W and the normalized length L/W of the ridge. In particular, we

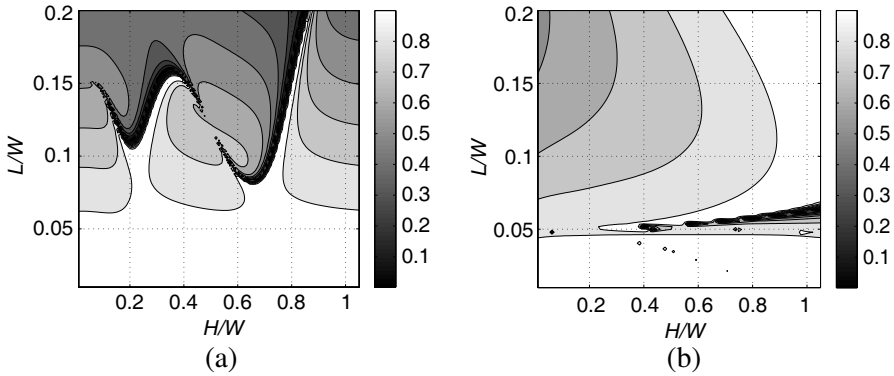

Figure 5. The magnitude of: the transmission coefficient for: (a) $\epsilon_{rx} = 2.5$, $\epsilon_{ry} = -3.5$, $\mu_r = 2.5$ and (b) $\epsilon_{rx} = 0.1$, $\epsilon_{ry} = 10$, $\mu_r = 1$ in contour plot with respect to the normalized depth $H = W$ and the normalized length $L = W$ of the well. Plot parameters: $W = 20\,\text{mm}$, $f = 0.8\frac{c}{2W}$.

consider a filling material with a hyperbolic dispersion relation [40]. It is clear that for fairly small horizontal dimension L/W, the response of the device is very weakly dependent on H/W and possesses substantial values. On average, the transfer function declines for increasing L/W, while there are certain lines on the (H/W, L/W) map that the represented quantity exhibits a dramatic variation. This feature could be proved useful when calibrating the optimal size of the device as it provides the designer with many different combinations of dimensions with high selectivity. In Figure 5(b), we show another contour plot of $|S_{21}|$ for the case of a typical anisotropic material. Again, considerable and uniform outputs for small L/W are recorded, while increasing H/W causes larger responses when L/W is not negligible. Therefore, another controlling characteristic of the parameter H/W becomes evident.

4. CONCLUDING REMARKS

A simple discontinuous waveguide with a narrow rectangular ridge filled with an anisotropic electromagnetic substance is examined as a two-port network. The solution is obtained with proper particularization of the mode matching technique and verified for its correctness. The discussed diagrams and graphs reveal interesting and potentially applicable features of the device related to high selectivity and easy controllability of the acquired response.

An interesting expansion of the aforementioned approach would be to add several degrees of freedom in the considered configuration that would improve the selectivity characteristics of the waveguide reaction. In particular, the filling material could be replaced by an inhomogeneous anisotropic medium and the discontinuity could have an arbitrary shape. Also, inserting periodically small scatterers inside the host material of the well, could render the structure more effective.

REFERENCES

1. Marrocco, G., "Pervasive electromagnetics: Sensing paradigms by passive RFID technology," *IEEE Wireless Communications*, Vol. 17, 2823–2827, 2010.
2. Dimitriou, A. G., A. Bletsas, and J. N. Sahalos, "On the design of passive RFID tags for ASK modulation," *Proceedings of the 5th European Conference on Antennas and Propagation (EuCAP 2011)*, Rome, April 11–15, 2011.
3. Shaker, G., S. Safavi-Naeini, N. Sangary, and M. M. Tentzeris, "Inkjet printing of ultrawideband (UWB) antennas on paper-

based substrates," *IEEE Antennas and Wireless Propagation Letters*, Vol. 10, 111–114, 2011.

4. Weng, M. H., C.-H. Kao, and Y.-C. Chang, "A compact dual-band bandpass filter with high band selectivity using cross-coupled asymmetric SIRs for WLANs," *Journal of Electromagnetic Waves and Applications*, Vol. 24, No. 2–3, 161–168, 2010.
5. Xue, J.-Y., S.-X. Gong, P.-F. Zhang, W. Wang, and F.-F. Zhang, "A new miniaturized fractal frequency selective surface with excellent angular stability," *Progress In Electromagnetics Research Letters*, Vol. 13, 131–138, 2010.
6. Guo, C., H.-J. Sun, and X. Lv, "A novel dualband frequency selective surface with periodic cell perturbation," *Progress In Electromagnetics Research B*, Vol. 9, 137–149, 2008.
7. Chen, J., S. Quegan, and X. Yin, "Calibration of spaceborne linearly polarized low frequency SAR using polarimetric selective radar calibrators," *Progress In Electromagnetics Research*, Vol. 114, 89–111, 2011.
8. Zhang, J.-C., Y.-Z. Yin, and J.-P. Ma, "Design of narrow bandpass frequency selective surfaces for millimeter wave applications," *Progress In Electromagnetics Research*, Vol. 96, 287–298, 2009.
9. Zhu, Y. Z., H. S. Song, and K. Guan, "Design of optimized selective quasi-elliptic filters," *Journal of Electromagnetic Waves and Applications*, Vol. 23, No. 10, 1357–1366, 2009.
10. Karlsson, A., D. Sjoberg, and B. Widenberg, "Frequency selective structures with stochastic deviations," *Progress In Electromagnetics Research*, Vol. 74, 141–155, 2007.
11. Lin, X. Q., T. J. Cui, Y. Fan, and X. Liu, "Frequency selective surface designed using electric resonant structures in terahertz frequency bands," *Journal of Electromagnetic Waves and Applications*, Vol. 23, No. 1, 21–29, 2009.
12. Zhang, J.-C., Y.-Z. Yin, and J.-P. Ma, "Frequency selective surfaces with fractal four legged elements," *Progress In Electromagnetics Research Letters*, Vol. 8, 1–8, 2009.
13. Siddiqui, O. F. and O. M. Ramahi, "Frequency-selective energy tunneling in wire-loaded narrow waveguide channels," *Progress In Electromagnetics Research Letters*, Vol. 15, 153–161, 2010.
14. Belyaev, B. A., A. A. Leksikov, A. M. Serzhantov, and V. V. Tyurnev, "Highly selective suspended stripline dual-mode filter," *Progress In Electromagnetics Research Letters*, Vol. 25, 57–66, 2011.

15. Kawakatsu, M. N., V. A. Dmitriev, and S. L. Prosvirnin, "Microwave frequency selective surfaces with high Q-factor resonance and polarization insensitivity," *Journal of Electromagnetic Waves and Applications*, Vol. 24, No. 2–3, 261–270, 2010.
16. Jiao, C.-Q., "Selective suppression of electromagnetic modes in a rectangular waveguide by using distributed wall losses," *Progress In Electromagnetics Research Letters*, Vol. 22, 119–128, 2011.
17. Islam, S., J. Stiens, G. Poesen, R. Vounckx, J. Peeters, I. Bogaert, D. De Zutter, and W. De Raedt, "Simulation and experimental verification of w-band finite frequency selective surfaces on infinite background with 3D full wave solver NSPWMLFMA," *Progress In Electromagnetics Research*, Vol. 101, 189–202, 2010.
18. Ucar, M. H. B., A. Sondas, and Y. E. Erdemli, "Switchable split-ring frequency selective," *Progress In Electromagnetics Research B*, Vol. 6, 65–79, 2008.
19. Coombs, C. F., *Printed Circuits Handbook*, McGraw-Hill Professional, 1.3–3.29, 2001.
20. Shestopalov, V. P., A. A. Kirilenko, and L. A. Rud, *Resonance Wave Scattering*, Vol. 2, Waveguide Discontinuities, 1986 (in Russian).
21. Valagiannopoulos, C. A., "Rigorous analysis of a metallic circular post in a rectangular waveguide with step discontinuity of sidewalls," *IEEE Transactions on Microwave Theory and Techniques*, Vol. 55, 2007.
22. Valagiannopoulos, C. A. and N. K. Uzunoglu, "Green's function of a parallel plate waveguide with multiple abrupt changes of interwall distances," *Radio Science*, Vol. 44, 2009.
23. Valagiannopoulos, C. A., "Arbitrary currents on circular cylinder with inhomogeneous cladding and RCS optimization," *Journal of Electromagnetic Waves and Applications*, Vol. 21, No. 5, 665–680, 2007.
24. Valagiannopoulos, C. A., "Effect of cylindrical scatterer with arbitrary curvature on the features of a metamaterial slab antenna," *Progress In Electromagnetics Research*, Vol. 71, 59–83, 2007.
25. Zhang, H.-W., X.-W. Zhao, Y. Zhang, D. G. Donoro, W. X. Zhao, and C. H. Liang, "Analysis of a large scale narrow-wall slotted waveguide array by parallel MoM out-of-core solver using the higher order basis functions," *Journal of Electromagnetic Waves and Applications*, Vol. 24, No. 14–15, 1953–1965, 2010.

26. Valagiannopoulos, C. A., "Single-series solution to the radiation of loop antenna in the presence of a conducting sphere," *Progress In Electromagnetics Research*, Vol. 71, 277–294, 2007.
27. Valagiannopoulos, C. A., "An overview of the Watson transformation presented through a simple example," *Progress In Electromagnetics Research*, Vol. 75, 137–152, 2007.
28. Park, G. H. and Y. B. Park, "Capacitance of asymmetric conductor-backed coplanar waveguides," *Journal of Electromagnetic Waves and Applications*, Vol. 24, No. 13, 1721–1729, 2010.
29. Valagiannopoulos, C. A., "Closed-form solution to the scattering of a skew strip field by metallic pin in a slab," *Progress In Electromagnetics Research*, Vol. 79, 1–21, 2008.
30. Valagiannopoulos, C. A., "Electromagnetic scattering from two eccentric metamaterial cylinders with frequency-dependent permittivities differing slightly each other," *Progress In Electromagnetics Research B*, Vol. 3, 23–34, 2008.
31. Shen, W., W.-Y. Yin, X.-W. Sun, and J.-F. Mao, "Compact coplanar waveguide-incorporated substrate integrated waveguide (SIW) filter," *Journal of Electromagnetic Waves and Applications*, Vol. 24, No. 7, 871–879, 2010.
32. Valagiannopoulos, C. A., "On measuring the permittivity tensor of an anisotropic material from the transmission coefficients," *Progress In Electromagnetics Research B*, Vol. 9, 105–116, 2008.
33. Valagiannopoulos, C. A., "A Novel methodology for estimating the permittivity of a specimen rod at low radio frequencies," *Journal of Electromagnetic Waves and Applications*, Vol. 24, No. 5–6, 631–640, 2010.
34. Khalilpour, J. and M. Hakkak, "Controllable waveguide bandstop filter using S-shaped ring resonators," *Journal of Electromagnetic Waves and Applications*, Vol. 24, No. 5–6, 587–596, 2010.
35. Valagiannopoulos, C. A., "On developing alternating voltage around a rotating circular ring under plane wave excitation in the presence of an eccentrically positioned metallic core," *Progress In Electromagnetics Research M*, Vol. 12, 193–204, 2010.
36. Valagiannopoulos, C. A., "Electromagnetic scattering of the field of a metamaterial slab antenna by an arbitrarily positioned cluster of metallic cylinders," *Progress In Electromagnetics Research*, Vol. 114, 51–66, 2011.
37. Zhang, H., S. Yim, T. Hong, and S. Tan, "Experimental investigation on flanged parallel-plate dielectric waveguide probe for detection of conductive inclusions in lossy dielectric medium,"

Journal of Electromagnetic Waves and Applications, Vol. 24, No. 5–6, 681–693, 2010.

38. Valagiannopoulos, C. A., "A signal coverage model for two neighboring islands of different size," *Progress In Electromagnetics Research M*, Vol. 2, 115–130, 2008.
39. Valagiannopoulos, C. A., "On examining the influence of a thin dielectric strip posed across the diameter of a penetrable radiating cylinder," *Progress In Electromagnetics Research C*, Vol. 3, 203–214, 2008.
40. Valagiannopoulos, C. A. and C. R. Simovski, "Conversion of evanescent waves into propagating modes by passing through a metamaterial prism: An iterative approximation method," *Proceedings of the 5th European Conference on Antennas and Propagation (EuCAP 2011)*, Rome, April 11–15, 2011.
41. Orphanidis, S. J., *Electromagnetic Waves and Antennas*, freely available online at: http://eceweb1.rutgers.edu/∼orfanidi/ewa, Vol. 13, 530–533, 2008.
42. Alù, A., M. G. Silveirinha, A. Salandrino, and N. Engheta, "Epsilon-near-zero metamaterials and electromagnetic sources: tailoring the radiation phase pattern," *Physical Review B*, Vol. 75, 155410, 2007.
43. Valagiannopoulos, C. A. and N. K. Uzunoglu, "Scattering of ELF waves by underground formations because of night-day ionospheric ridge," *Radio Science*, Vol. 42, RS6S32, 2007.
44. Valagiannopoulos, C. A., "Study of an electrically anisotropic cylinder excited magnetically by a straight strip line," *Progress In Electromagnetics Research*, Vol. 73, 297–325, 2007.